

# Phase Measurements in Aharonov-Bohm Interferometers

Amnon AHARONY<sup>1</sup>, Ora ENTIN-WOHLMAN<sup>1</sup>, Yoseph IMRY<sup>2</sup>

<sup>1</sup>*School of Physics and Astronomy, Raymond and Beverly Sackler Faculty of Exact Sciences,  
Tel Aviv University, Tel Aviv 69978, ISRAEL*

<sup>2</sup>*Department of Condensed Matter Physics, The Weizmann Institute of Science, Rehovot 76100, ISRAEL*

Received 28.08.2003

## Abstract

In this paper we address measurements of the resonant quantum transmission amplitude  $t_{QD} = -i|t_{QD}|e^{i\alpha_{QD}}$  through a quantum dot (QD), as function of the plunger gate voltage  $V$ . Mesoscopic solid state Aharonov-Bohm interferometers (ABI) have been used to measure the “intrinsic” phase,  $\alpha_{QD}$ , when the QD is placed on one of the paths. In a “closed” interferometer, connected to two terminals, the electron current is conserved, and Onsager’s relations require that the conductance  $\mathcal{G}$  through the ABI is an even function of the magnetic flux  $\Phi = \hbar c\phi/e$  threading the ABI ring. Therefore, if one fits  $\mathcal{G}$  to  $A + B\cos(\phi + \beta)$  then  $\beta$  only “jumps” between 0 and  $\pi$ , with no relation to  $\alpha_{QD}$ . Additional terminals open the ABI, break the Onsager relations and yield a non-trivial variation of  $\beta$  with  $V$ . After reviewing these topics, we use theoretical models to derive three results on this problem: (i) For the one-dimensional leads, the relation  $|t_{QD}|^2 \propto \sin^2(\alpha_{QD})$  allows a direct measurement of  $\alpha_{QD}$ . (ii) In many cases, the measured  $\mathcal{G}$  in the closed ABI can be used to extract *both*  $|t_{QD}|$  and  $\alpha_{QD}$ . (iii) For open ABI’s,  $\beta$  depends on the details of the opening. We present quantitative criteria (which can be tested experimentally) for  $\beta$  to be equal to the desired  $\alpha_{QD}$ : the “lossy” channels near the QD should have both a small transmission and a small reflection.

**Key Words:** interference in nanostructures, Aharonov-Bohm interferometer, quantum dots, resonant transmission.

## 1. Introduction and Review of Experiments

Recent advances in the fabrication of nanometer scale electronic devices raised much interest in the quantum mechanics of quantum dots (QDs), which represent artificial atoms with experimentally controllable properties [1, 2]. A flexible method to construct mesoscopic QDs is based on the two dimensional electron gas (2DEG), which exists in the planar interface between an insulator and a semiconductor, with a metallic layer under the insulator. Metallic electrodes, which are placed above the semiconducting layer, create potentials on the 2DEG which restrict the electrons to move only in parts of the plane [3]. The simplest QD geometry consists of a small bounded region, which can bind electrons. This QD is connected via two one-dimensional (1D) ‘metallic’ leads to electron reservoirs. The coupling of each lead to the QD is controlled by a potential barrier. The potential on the QD itself, called the ‘plunger gate voltage’,  $V$ , determines the attraction of electrons to the QD, and thus also the energies of electronic bound states on the QD. The simplest experiments then measure the conductance  $\mathcal{G}$  through the QD, as function of  $V$ . The measured  $\mathcal{G}$  shows peaks whenever the Fermi energy  $\epsilon_F$  of the electrons crosses a bound state on the QD. Quantum mechanically, we should think of an electronic wave,  $e^{ikx}$ , hitting the QD from the left. One then ends up with a reflected wave,  $r_{QD}e^{-ikx}$  and a transmitted wave,  $t_{QD}e^{ikx}$ . The quantum information on the resonant

tunneling through the QD is contained in the *complex* transmission amplitude,  $t_{QD} = -i\sqrt{\mathcal{T}_{QD}}e^{i\alpha_{QD}}$ . It is thus of great interest to measure both the magnitude  $\mathcal{T}_{QD}$  and the phase  $\alpha_{QD}$ , and study their dependence on  $V$ .

Theoretically, the phase  $\alpha_{QD}$  is particularly interesting, given its relation to the additional electron occupation in the system via the Friedel sum rule [4, 5]. This phase is also predicted to exhibit interesting behavior e.g. near a Kondo-like resonance [6]. For a simple model of non-interacting electrons with several equidistant bound state energies, theory yields the magnitude and the phase as shown in Fig. 1 (see below for details):  $\mathcal{T}_{QD}$  exhibits resonances at the bound state energies, while  $\alpha_{QD}$  exhibits an interesting variation between 0 and  $\pi$ , growing gradually through each resonance, and dropping sharply between consecutive resonances (here and in all following graphs, we set  $\alpha$  and  $\beta$  at zero far below the resonances). The resonant dependence of  $\mathcal{T}_{QD}$  on  $V$  has been confirmed by many experiments [1, 2], which measure the conductance and take advantage of the Landauer formula [7],  $\mathcal{G} = \frac{2e^2}{h}\mathcal{T}_{QD}$ . However, the experimental measurement of  $\alpha_{QD}$  has only become accessible since 1995 [8, 9], using the Aharonov-Bohm (AB) interferometer [10]. As explained below, many experiments measure a phase (which we call  $\beta$ ) which 'oscillates' between 0 and  $\pi$ . However, the relation of these measured values to the desired  $\alpha_{QD}$  is not trivial. This relation is one of the main topics of this review.

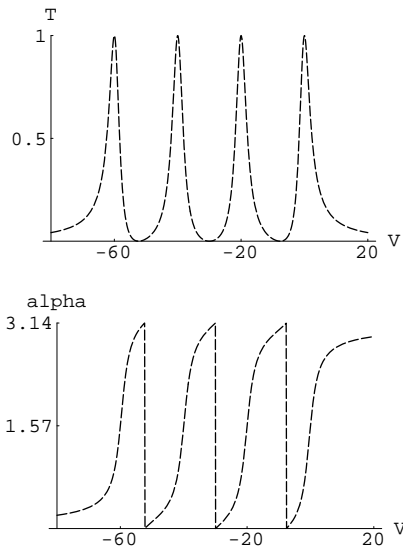


**Figure 1.** Theoretical transmission  $\mathcal{T}_{QD}$  and “intrinsic” phase  $\alpha_{QD}$  for  $N = 4$  states on the QD, with “gap”  $U = 20J$ , versus the gate voltage  $V$  (in units of  $J$ ). See Sec. 2 for details.

The simplest method to measure the phase of a wave is based on the *two-slit interferometer* [11]. In this geometry, a coherent electron beam is split between two paths, going through two slits, and one measures the distribution of electrons absorbed on a screen behind the two slits. Assuming that each electron goes through one of the slits only *once*, without any reflection from the slits or from the screen, and assuming complete coherence, the distribution of electrons on the screen is given by  $\mathcal{T} = |t|^2$ , where  $t = t_1 + t_2$  is the sum of the (complex) amplitudes of the waves which went via the two slits.

In the two-slit AB interferometer, one adds a magnetic flux  $\Phi$  in the area surrounded by the two electronic paths. Such a flux creates a non-zero electromagnetic vector potential,  $\mathbf{A}$ , even where the flux vanishes. With an appropriate choice of gauge, the kinetic energy of the electron becomes  $(\mathbf{p} + e\mathbf{A}/c)^2/(2m)$ , where  $\mathbf{p}$  is the electron momentum. As a result, the wave function of the free electron which moves from  $\mathbf{r}_1$  to  $\mathbf{r}_2$  obtains an additional phase  $\phi_{12} = (e/\hbar c) \int_{\mathbf{r}_1}^{\mathbf{r}_2} \mathbf{A}(\mathbf{r}) \cdot d\mathbf{r}$ , where the integration is along the path of the electron. Aharonov and Bohm [12] used this fact to predict that such a flux between the two paths would

add a difference  $\phi = e\Phi/\hbar c$  between the phases of the wave functions in the two branches of the ring, yielding

$$t = t_1 e^{i\phi} + t_2. \quad (1)$$

(Gauge invariance allows one to attach the AB phase  $\phi$  to either branch). Writing  $t_i = |t_i| e^{i\alpha_i}$ , one thus has

$$\mathcal{T} = A + B \cos(\phi + \alpha), \quad (2)$$

where  $\alpha = \alpha_1 - \alpha_2$ . Assuming that one of the phases can be varied experimentally (e.g. by placing a QD on one path and changing its plunger gate voltage  $V$ ), this ‘2-slit formula’ can then be used to deduce the dependence of the phase  $\alpha$  on external parameters (e.g.  $V$ ).

Experiments using two-slit geometries for electron interference, using electron microscopes, which confirmed the AB effect, have been described in detail by Tonomura [13]. In the present paper we concentrate on experiments which use *mesoscopic devices*. A coherent flow of electrons requires that the mean free path  $L_\varphi$ , over which scattering destroys the electron’s phase, should be larger than the sample size. This can be achieved by going to low temperatures and by using small samples. The first confirmation of the AB effect in a mesoscopic system was done by Webb *et al.* [14]. They used a small metal ring, which was connected (at two opposite points) to electron reservoirs through two leads. Indeed, the conductance of the ring showed a periodic dependence on the magnetic flux inside the ring,  $\Phi$ , with a leading Fourier component at the period  $e/\hbar c$ , as expected. However, this experiment did not allow a variation of the relative phase  $\alpha$ , nor a detailed test of the two-slit formula (2); specifically, the Fourier analysis contained also higher harmonics.

The first attempt to vary the phase of the wave on one of the paths was done by Yacoby *et al.* [8]. They used the semiconducting QD system described above, in which the electrons were also allowed to go via a ‘reference’ path, parallel to the path containing the QD (see Fig. 2a). Again, the measured conductance was periodic in  $\phi$ , and the detailed dependence of  $\mathcal{G}$  on  $\phi$  varied with the plunger gate voltage on the QD,  $V$ . Far away from a resonance, this conductance could be fitted to Eq. (2). However, closer to a resonance the data seem to require more harmonics in  $\phi$ , e.g. of the form

$$\mathcal{T} = A + B \cos(\phi + \beta) + C \cos(2\phi + \gamma) + \dots, \quad (3)$$

with the conventions  $B, C > 0$ . Surprisingly, the fitted phase  $\beta$  did not vary continuously with  $V$  (as would be implied from the 2-slit scenario and Eq. (2)). Instead,  $\beta$  remained fixed between resonances, with only discrete jumps by  $+\pi$  (near a resonance) or by  $-\pi$  (between resonances). These discrete jumps are definitely different from the behavior of the intrinsic phase  $\alpha_{QD}$ , as shown e.g. in Fig. 1. Therefore, these experiments cannot be used for direct measurements of  $\alpha_{QD}$ , using Eq. (2) or Eq. (3).

The reason for this discrepancy was soon understood. Both the experiments by Webb *et al.* and by Yacoby *et al.* were done on ‘closed’ interferometers, which differ significantly from the two-slit geometry. Unlike the latter, the former require many reflections of the electron waves from the ‘forks’ connecting the ring with the leads; there is no way to write a  $3 \times 3$  unitary matrix, which contains no reflections in two of the three channels. Each such reflection adds a term to the interference sum of amplitudes, and modifies the simple two-slit formula. In fact, it was already shown by Onsager [15, 16] that unitarity (conservation of current) and time reversal symmetry imply that  $\mathcal{G}(\phi) = \mathcal{G}(-\phi)$ , and therefore  $\beta$  (as well as  $\gamma$  etc.) *must* be equal to zero or  $\pi$ , as observed by Yacoby *et al.*. Given the Onsager relation, it is clear that the data from the closed interferometer should not be analyzed using the two-slit formula (2). However, we show below that there exists a more complicated formula, which contains the many reflections from the ‘forks’, and that this formula can be used to extract the phase  $\alpha_{QD}$  from the closed interferometer data [17].

Later experiments [9] opened the interferometer, using the six-terminal configuration shown schematically in Fig. 2(b); the additional leads allow losses of electronic current, thus breaking unitarity. Indeed, fitting the conductance to Eq. (2) yielded a phase  $\beta$  which was qualitatively similar to the calculated  $\alpha_{QD}$ , as shown in Fig. 1: a gradual increase through each resonance (accompanied by peaks in the amplitudes  $A$  and  $B$ ), and a sharp ‘phase lapse’ back to zero between resonances (accompanied by zeroes in  $B$ ). These experimental results led to much theoretical discussion. Some of this [18, 19] emphasized the non-trivial effects of the ring itself on the measured results, even for the closed case. Other theoretical papers [20, 21, 22, 23, 24, 25, 26] *assumed* that the measured  $\beta$  represents the correct  $\alpha_{QD}$ , and discussed the possible origins of the observed features, e.g. the ‘phase lapse’ and the similarity between the data at many resonances. However, until

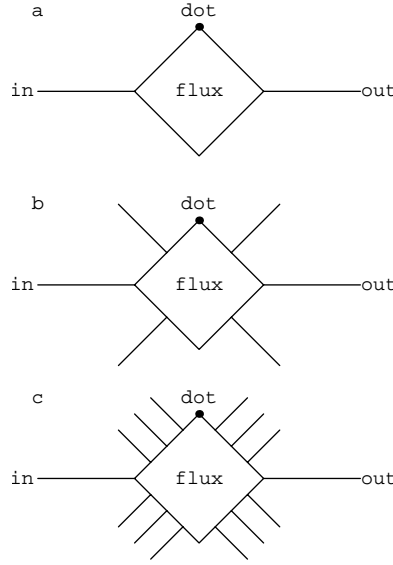


**Figure 2.** Model for the AB interferometer: (a) Closed two-terminal case, (b) Schematic picture of the six-terminal open interferometer, (c) Model for the open interferometer.

recently there existed no quantitative comparison of the measured  $\beta$  with the ‘intrinsic’  $\alpha_{QD}$ . In fact, as explained below, it turns out that  $\beta$  depends on the strength of the coupling to the open channels: when this coupling vanishes (in the ‘closed’ limit),  $\beta$  jumps between zero and  $\pi$ . As the coupling increases, the increase of  $\beta$  near a resonance becomes less steep, with a slope that decreases with increasing coupling [27]. Thus, it is not enough to open the interferometer; one also needs to choose specific methods of opening, and to tune the relevant parameters! Below we present a theoretical model, aimed to imitate the experimental setups of Fig. 2(a) and (b) [28]. It has been found that the two-slit conditions can be imitated if one replaces each lossy channel in Fig. 2(b) by many such channels, as illustrated in Fig. 2(c). Figure 3 shows examples of our model calculations for  $A$ ,  $B$ ,  $C$  and  $\beta$  versus  $V$ . Qualitatively, these plots look similar to those found experimentally [8, 9]. However, as discussed below, the quantitative results for the open interferometers depend on details of the opening.

## 2. Models for the QD

We demonstrate our results for a simple lattice model, in which the dot is represented by a single site “ $D$ ” (located at the origin), on a 1D tight binding chain [29]. All the on-site energies are zero, except  $\epsilon_D$  on the QD.  $\epsilon_D$  can be varied experimentally by the plunger gate voltage  $V$ . As usual for such models, electron-electron interactions are included only via an on-site Hubbard interaction  $U$  on the QD. The hopping matrix elements  $J_{i,i+1}$  on the chain are all equal to  $J$ , except on the bonds connected to the QD, where they are  $J_{-1,D} = J_L$  and  $J_{D,1} = J_R$ . Our Hamiltonian is thus given by

$$\mathcal{H}_0 = \sum_{\sigma} \left( \epsilon_D d_{\sigma}^{\dagger} d_{\sigma} + \frac{U}{2} n_{d\sigma} n_{d\bar{\sigma}} - J \sum_{i \neq -1,0} [c_{(i+1)\sigma}^{\dagger} c_{i\sigma} + h.c.] - [J_L d_{\sigma}^{\dagger} c_{-1\sigma} + J_R c_{1\sigma}^{\dagger} d_{\sigma} + h.c.] \right), \quad (4)$$

where  $c_{i\sigma}^{\dagger}$  creates an electron (with spin  $\sigma$ ) on site  $i$ . For the unperturbed chain (with  $\epsilon_D = 0$ ,  $U = 0$  and  $J_L = J_R = J$ ), one has simple wave eigenstates, with wave vectors  $k$  and eigenenergies  $\epsilon_k = -2J \cos ka$  ( $a$  is the lattice constant). The operators on the dot,  $d_{\sigma}$  and  $d_{\sigma}^{\dagger}$ , anti-commute with  $c_{i\sigma}$ ,  $c_{i\sigma}^{\dagger}$ . Also,  $n_{d\sigma} = d_{\sigma}^{\dagger} d_{\sigma}$ , and  $\bar{\sigma} \equiv -\sigma$ .

Adapting the results of Ref. [29], the transmission amplitude through the QD at zero temperature is

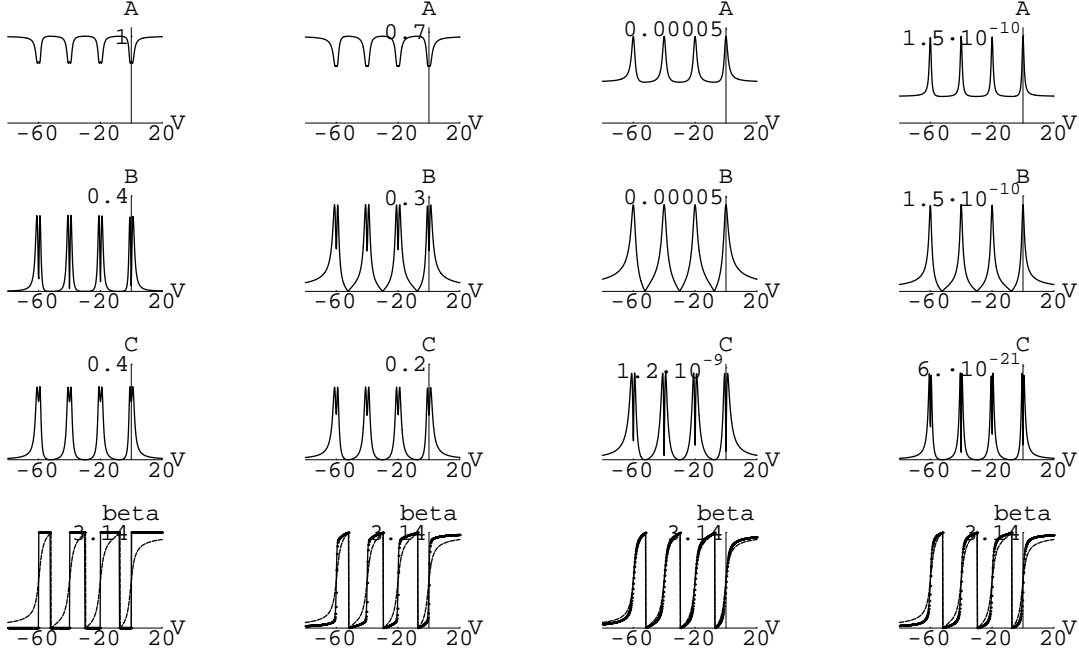


**Figure 3.**  $A$ ,  $B$ ,  $C$  and  $\beta$  for transmission through the closed AB ring (upper left), and for the open interferometer with  $J_x = .15J$  (upper right) and  $J_x = .9J$ ,  $1.5J$  (lower left, right). The dashed line shows the exact intrinsic phase  $\alpha_{QD}$ , from Fig. 1. For details see Sec. 4 below.

given by

$$t_{QD} = -i\gamma_D \sin \alpha_{QD} e^{i\alpha_{QD}} \equiv 2i \sin |k| a J_L J_R g_D(\epsilon_k) / J, \quad (5)$$

with the QD asymmetry factor  $\gamma_D = 2J_L J_R / (J_L^2 + J_R^2)$  and the “intrinsic” Green function on the QD,  $g_D(\epsilon_k) = 1/[\epsilon_k - \epsilon_D - \Sigma_D(\epsilon_k)]$ . Here,  $\Sigma_D(\epsilon_k)$  is the self-energy on the QD, which contains contributions from the leads,  $\Sigma_{D,ext} = -e^{ik|a|} (J_L^2 + J_R^2) / J$  (which exists also for the non-interacting case [27]), and from the electron-electron interactions on the QD itself,  $\Sigma_{D,int}(\omega)$  (which vanishes when  $U = 0$ ). As  $\epsilon_D \equiv V$  increases,  $\alpha_{QD}$  grows gradually from zero (far below the resonance), through  $\pi/2$  (at the resonance), towards  $\pi$  (far above the resonance).

Interestingly, for this one-dimensional model, normalizing the measured

$$\mathcal{T}_{QD} = |t_{QD}|^2 = \gamma_D^2 \sin^2(\alpha_{QD}) \quad (6)$$

by its ( $V$ -independent) maximum  $\max[\mathcal{T}_{QD}] \equiv \gamma_D^2$  yields the value of  $\alpha_{QD}$ . Assuming coherence, this method for measuring  $\alpha_{QD}$  directly from  $\mathcal{T}_{QD}$  eliminates the need for any complicated interferometry! (However, interferometry is still important, since it ensures coherence. Interestingly, this conclusion holds for any Breit-Wigner-like resonance, with an energy-independent width. It also holds for a multi-level QD, with many resonances). In the next section we discuss ways of extracting  $\alpha_{QD}$  indirectly, from the closed AB interferometer measurements. Comparing results from  $\sin^2(\alpha_{QD}) = \mathcal{T}_{QD} / \gamma_D^2 \equiv \mathcal{T}_{QD} / \max[\mathcal{T}_{QD}]$ , from the closed interferometer [17] and from the open one [28] (all with the same QD) should serve as consistency checks for this conclusion.

As explained above, at  $T = 0$  the ‘intrinsic’ transmission amplitude and phase are directly related to the ‘bare’ Green function  $g_D$  at the Fermi energy,  $\epsilon_F$ , which is equal to  $\epsilon_k$ . Explicit calculations of this Green function, in the presence of interactions, are non trivial. Although some of the results below will be given in terms of the full Green function, it is often useful to use simple expressions to illustrate specific points. For such purposes, in some of the explicit calculations below we follow many earlier calculations

[18, 26, 30, 31, 32], and ignore the interactions. For  $U = 0$ , we end up with a simple single-electron tight-binding model. In this case, the Schrödinger wave equation is written as  $(E - \epsilon_i)\psi_i = -\sum_j J_{ij}\psi_j$ , where the sum is over nearest neighbors of  $i$ . The scattering solution for a wave coming from the left, with wave vector  $k$  and energy  $E = -2J \cos ka$ , is described by  $\psi_m^L = e^{ikam} + r e^{-ikam}$  on the left, and by  $\psi_m^R = t e^{ikam}$  on the right. The calculation of the transmission and reflection amplitudes,  $t$  and  $r$ , then amounts to solving a finite set of linear equations for the wave functions inside the scatterer.

Similar linear equations arise for single electron scattering from more complex geometries, like those shown in Fig. 2. In each such calculation, we have a scattering element (e.g. the ‘ring’) connected to two one-dimensional (1D) leads, which have  $J_{i,i+1} = J$ ,  $\epsilon_i = 0$ . All the explicit graphs presented in the paper are based on the extraction of the total transmission amplitude  $t$  from such equations.

As discussed above, in many cases one is interested in dots which have more than one resonance. Without interactions, it is easy to generalize the above tight-binding model to a QD with many discrete energy levels. This is done by a set of smaller dots, each containing a single resonant state, with energy  $\{\epsilon_D = E_R(n), n = 1, \dots, N\}$ . This model is shown in Fig. 4 for  $N = 4$ . Each such state (or small dot) is connected to its left and right nearest neighbors on the leads via bonds with hopping amplitudes  $\{J_L(n), J_R(n), n = 1, \dots, N\}$ . The QD can thus be described by  $N$  wave functions  $\psi_n$ , obeying  $[E - E_R(n)]\psi_n = -J_L(n)\psi_0^L - J_R(n)\psi_0^R$  (where we choose  $\psi_0^L = 1 + r$ ,  $\psi_0^R = t$ ). The exact transmission amplitude is easily found to be

$$t_{QD} = \frac{S_{LR} 2i \sin ka}{(S_{LL} + e^{-ika})(S_{RR} + e^{-ika}) - |S_{LR}|^2}, \quad (7)$$

where

$$S_{XY} = \sum_n \frac{J_X(n) J_Y(n)^*}{J[E - E_R(n)]}, \quad X, Y = L, R \quad (8)$$

represent ‘bare’ Green’s functions for sites  $L$  and  $R$  (in the previous notation, these were sites  $-1$  and  $1$  on the chain).

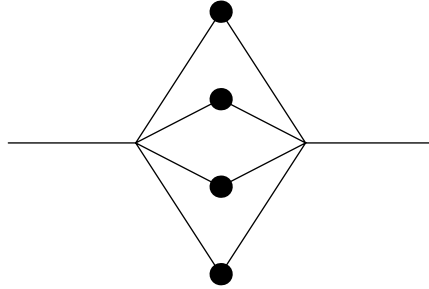


**Figure 4.** Model for a QD with four discrete energy levels.

Figure 1 was generated by Eq. (7), with equidistant bound state energies,  $E_R(n) = V + U(n - 1)$ . The ‘gap’  $U$  can be viewed as the Hartree energy for an electron added to a QD which already has  $n - 1$  other electrons [20], thus capturing some aspects of the **Coulomb blockade** behavior of the scattered electron. We study  $t_{QD}$  as function of the energy  $V$ , which represents the plunger gate voltage on the QD. In this figure and below, we choose  $ka = \pi/2$ , so that  $E = 0$  and the resonances of the transmission, where  $T_{QD} = 1$ , occur exactly when  $E_R(n) = E = 0$ , i.e. when  $V = -U(n - 1)$  [33]. Results are not sensitive to  $k$  near the band center. We also use the simple symmetric case,  $J_L(n) = J_R(n) \equiv J$ , and measure all energies in units of  $J$ . As mentioned, this model reproduces the apparently observed behavior of  $\alpha_{QD}$ : it grows smoothly from 0 to  $\pi$  as  $E$  crosses  $E_R(n)$ , and exhibits a sharp ‘phase lapse’ from  $\pi$  to 0 between neighboring resonances, at points where  $T_{QD} = 0$ . These latter points, associated with zeroes of  $S_{LR}$ , represent Fano-like destructive interference between the states on the QD [35, 22, 23, 34, 36].

In fact, Eq. (7) gives an excellent approximant for the scattering through a general QD, with several competing resonances. In Fig. 5 we present results for the transmission through such a QD, with an

appropriate (non-symmetric) choice of the parameters  $\{E_R(n), J_L(n)$  and  $J_R(n)\}$ , and  $N = 5$ . This figure reproduces all the experimental features observed by Göres *et al.* [37], in scattering from a single electron transistor. Clearly, our Eq. (7) gives a much better description of the data, with less parameters, compared to the sum of individual non-symmetric Fano expressions [35] used in Ref. [37] to fit the experiments.

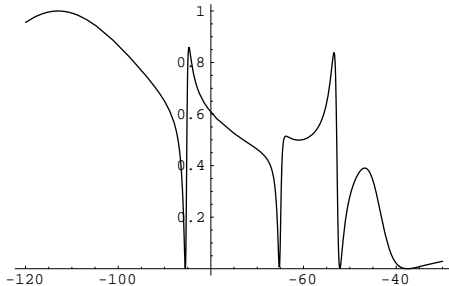


**Figure 5.** Conductance versus gate voltage for a model of a single electron transistor, based on Eq. (7).

Many earlier theoretical (e.g. [20]) and experimental (e.g. [9]) papers approximated  $t$  by a sum of the single resonance Breit-Wigner-like (BW) expressions [38],

$$t_{QD} \approx \sum_n \frac{e^{2ika} 2i \sin ka J_L(n) J_R(n)^*}{E - E_R(n) + e^{ika} [ |J_L(n)|^2 + |J_R(n)|^2 ] / J}. \quad (9)$$

Each term here has the form of Eq. (5), apart from a trivial overall phase factor  $e^{2ika}$ . Although this form gives an excellent approximation for  $t_{QD}$  near each resonance, it completely misses the Fano-like zeroes and the “phase lapses” between resonances. This happens because the approximation moves the zeroes off the real energy axis [34]. As a result, the approximate  $\alpha_{QD}$  never reaches 0 or  $\pi$ , and exhibits a smooth decrease from a maximum to a minimum near the correct “phase lapse” values of  $V$ . Since our aim here is to check on accurate measurements of the “intrinsic” phase, for a broad range of the parameters, and since the phase lapse has been a topic of much recent discussion [20, 21, 22, 23, 24, 25, 26], we prefer to use the exact solutions everywhere. This is particularly important since typically, available experimental data [9] show quite broad resonances, so that the BW approximation is bound to fail between them.

We emphasize again: in spite of the close similarity of our “intrinsic” transmission results with the experiments, the purpose of this paper is not to relate the calculated  $t_{QD}$  to the experimental systems. This would require a justification for our choice of the same  $J_L(n)$ ’s and  $J_R(n)$ ’s for all the resonances, which goes beyond the scope of the present paper. Rather, we aim to check when the AB interferometer reproduces the “input” behavior of the QD, by yielding  $\beta = \alpha_{QD}$  for all  $V$ . If this fails for our simple model then it would surely fail in the more complicated cases, where electron-electron interactions (beyond our simple Hartree approximation) become important [39].

### 3. Model for the closed AB interferometer

We next place the above QD on the upper branch of the closed AB interferometer, as shown in Fig. 2(a). In the context of our tight binding model, this translates into the model shown in Fig. 6: in addition to the path through the QD, we add a ‘reference’ path, which connects the left and right leads to the site ‘ref’ via matrix elements  $I_L$  and  $I_R$ . Ignoring electron interactions on this path, the new Hamiltonian becomes

$$\mathcal{H} = \mathcal{H}_0 + \sum_{\sigma} \left( \epsilon_0 c_{0\sigma}^{\dagger} c_{0\sigma} - I_L [c_{-1\sigma}^{\dagger} c_{0\sigma} + h.c.] - I_R [c_{0\sigma}^{\dagger} c_{1\sigma} + h.c.] \right). \quad (10)$$

The reference site energy  $\epsilon_0$  can be varied experimentally by an appropriately chosen gate voltage, which we denote by  $V_0$ . Adding a magnetic flux  $\Phi$  inside the AB ring now requires adding a phase  $\phi$  anywhere around the ring. Using gauge invariance, we do this by the replacement  $J_R \rightarrow J_R e^{i\phi}$ .

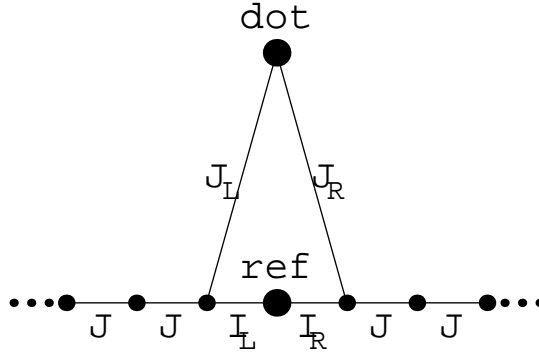


**Figure 6.** Model for the closed AB interferometer.

In principle, one can now start from the exact relation of Eq. (5), and add the effects of the ‘reference’ path perturbatively, as a power series in  $I_L$  and  $I_R$ . A more general approach uses the standard relation between the  $2 \times 2$  scattering matrix  $T_{kk'}$  and the matrix of retarded single-particle Green functions,  $G_{kk'}(\omega) = \delta_{kk'} g_k^0 + g_k^0 T_{kk'}^\sigma g_{k'}^0$ , with  $g_k^0(\omega) = 1/(\omega - \epsilon_k)$ , evaluated on the energy shell,  $\omega = \epsilon_F = \epsilon_k = \epsilon_{k'}$  [6]. The equation-of-motion (EOM) method [6] is then used to express  $(\omega - \epsilon_k)G_{kk'}(\omega)$  and  $(\omega - \epsilon_k)G_{kd}(\omega)$  as linear combinations of each other and of  $G_D(\omega)$ , allowing us to express each of them (and thus also  $t \propto T_{|k|,|k|}$ ) in terms of the Green function on the dot,  $G_D(\omega)$ . Since we do not use an explicit solution for  $G_D(\omega)$  itself, we don’t need to deal with the higher order correlation functions (due to  $U$ ), which appear in its EOM. The result of these procedures has the form [17]

$$t = A_D t_{QD} e^{i\phi} + A_B t_B, \quad (11)$$

where  $A_D = g_B(\epsilon_k - \epsilon_0)G_D(\epsilon_k)/g_D(\epsilon_k)$  and  $A_B = 1 + G_D(\epsilon_k)\Sigma_{ext}(\epsilon_k)$ . Here,  $G_D(\omega) = 1/[\omega - \epsilon_D - \Sigma(\omega)]$  is the fully “dressed” Green function on the QD, with the dressed self-energy  $\Sigma = \Sigma_{int} + \Sigma_{ext}$ . Both terms in  $\Sigma$  differ from their counterparts in the “intrinsic”  $\Sigma_D$ , by contributions due to the reference path. Also,

$$t_B = -i\gamma_B \sin \delta_B e^{i\delta_B} = 2i \sin |k| I_L I_R g_B / J \quad (12)$$

is the transmission amplitude of the “background”, or “reference”, path (when  $J_L = J_R = 0$ , or  $|\epsilon_D| \rightarrow \infty$ ), with the bare reference site Green function  $g_B = 1/[\epsilon_k - \epsilon_0 + e^{i|k|}(I_L^2 + I_R^2)/J]$ , and the asymmetry factor  $\gamma_B = 2I_L I_R / (I_L^2 + I_R^2)$ .

Equation (11) looks like the two-slit formula, Eq. (1). However, each of the terms is now *renormalized*:  $A_D$  contains all the additional processes in which the electron “visits” the reference site ( $A_D = 1$  when  $I_L = I_R = 0$ , or when  $|\epsilon_0| \rightarrow \infty$ ), and  $A_B$  contains the corrections to  $t_B$  due to “visits” on the dot. We now discuss the  $\phi$ -dependence of  $\mathcal{T} \equiv |t|^2$ , in connection with the Onsager relations and with the possible indirect extraction of  $\alpha_{QD}$ .

We first note that both parts in  $\Sigma(\epsilon_k)$  are *even* in  $\phi$ , due to additive contributions (with equal amplitudes) from clockwise and counterclockwise motions of the electron around the ring (see e.g. Refs. [10, 27, 30, 40]). In order that  $\mathcal{T}$  also depends only on  $\cos \phi$ , as required by the Onsager relations, the ratio  $K \equiv A_B t_B / (A_D t_{QD}) \equiv \tilde{x}[G_D(\epsilon_k)^{-1} + \Sigma_{ext}(\epsilon_k)]$ , with the real coefficient  $\tilde{x} = I_L I_R / [J_L J_R (\epsilon_k - \epsilon_0)]$ , must be real, i.e.

$$\Im[G_D(\epsilon_k)^{-1} + \Sigma_{ext}(\epsilon_k)] \equiv \Im \Sigma_{int} \equiv 0. \quad (13)$$

The same relation follows from the unitarity of the  $2 \times 2$  scattering matrix of the ring. This relation already appeared for the special case of single impurity scattering, in connection with the Friedel sum rule [5], and was implicitly contained in Eq. (5), where  $\Im \Sigma_{D,int} = 0$  [29]. Equation (13) implies that (at  $T = 0$  and  $\omega = \epsilon_k$ ) the *interaction self-energy*  $\Sigma_{int}(\epsilon_k)$  is *real*, and therefore the width of the resonance,  $\Im G_D(\epsilon_k)^{-1}$ , is *fully determined by the non-interacting self-energy*  $\Im \Sigma_{ext}(\epsilon_k)$ .

Since  $\Sigma_{ext}(\omega)$  depends only on the (non-interacting) tight-binding terms, it is easy to calculate it explicitly. We find  $\Sigma_{ext}(\epsilon_k) = \Sigma_{D,ext}(\epsilon_k) + \Delta_{ext}$ , where

$$\Delta_{ext} = e^{2i|k|} g_B (J_L^2 I_L^2 + J_R^2 I_R^2 + 2J_L J_R I_L I_R \cos \phi) / J^2. \quad (14)$$

The term proportional to  $\cos \phi$  comes from the electron clock- and counterclockwise motion around the AB “ring”. Similarly, one can write  $\Sigma_{int}(\epsilon_k) = \Sigma_{D,int}(\epsilon_k) + \Delta_{int}$ , and thus  $G_D(\epsilon_k)^{-1} = g_D(\epsilon_k)^{-1} - \Delta$ , with  $\Delta = \Delta_{ext} + \Delta_{int}$ . Hence,  $t = A_D t_D (e^{i\phi} + K)$ . Writing also  $A_D = C/[1 - g_D(\epsilon_k)\Delta]$ , with  $C = (\epsilon_k - \epsilon_0)g_B$ , we find

$$\mathcal{T} = |C|^2 \mathcal{T}_D \frac{1 + K^2 + 2K \cos \phi}{1 - 2\Re[g_D \Delta] + |g_D \Delta|^2}. \quad (15)$$

Although the numerator in Eq. (15) looks like the two-slit Eq. (1), with  $\beta = 0$  or  $\pi$  (depending on  $\text{sign}K$ ), the new physics is contained in the denominator – which becomes important in the vicinity of a resonance. The central term in this denominator depends explicitly on the phase of the complex number  $g_D$ . Since this number is directly related to  $t_{QD}$ , via Eq. (5), one may expect to extract  $\alpha_{QD}$  from a fit to Eq. (15), taking advantage of the dependence of the denominator on  $\cos \phi$ . Physically, this dependence originates from the infinite sum over electron paths which circulate the AB ring. Ref. [17] contains a detailed discussion of the conditions for such an extraction. Generally, this is not trivial, as one needs the detailed dependence of  $\Delta$  on  $\cos \phi$  and on the various parameters. We have presented this dependence for  $\Delta_{ext}$ , but not for  $\Delta_{int}$ .

The extraction of  $\alpha_{QD}$  becomes easy when one may neglect  $\Delta_{int}$ . The simplest case for this is for single-electron scattering, when  $\Sigma_{int} = 0$ . Interactions (i.e.  $U \neq 0$ ) are also negligible for a relatively *open* dot, with small barriers at its contacts with the leads [41]. Another effectively single-electron scattering case arises near a Coulomb blockade resonance, when the effect of interactions can simply be absorbed into a Hartree-like shift,  $\epsilon_D + \Sigma_{int} \rightarrow \epsilon_D + NU$ , if one *assumes* that  $N$  depends smoothly on the number of electrons on the QD, and not on  $\phi$  [40]. If one may neglect  $\Delta_{int}$ , then  $\Delta \approx \Delta_{ext}$  is given in Eq. (14). Using also Eqs. (5) and (12), we find

$$\mathcal{T} = |C|^2 \mathcal{T}_{QD} \frac{1 + K^2 + 2K \cos \phi}{1 + 2P(z + \cos \phi) + Q(z + \cos \phi)^2}, \quad (16)$$

where  $z = (J_L^2 I_L^2 + J_R^2 I_R^2) / (2J_L J_R I_L I_R)$ ,  $P = \Re[vt_B t_{QD}]$ ,  $Q = |vt_B|^2 \mathcal{T}_{QD}$ , and  $v = e^{2i|k|a} / (2 \sin^2 |k|a)$  depends only on the Fermi wavevector  $k$ , independent of any detail of the interferometer. A 5-parameter fit to the explicit  $\phi$ -dependence in Eq. (16) for given values of  $V$  and  $V_0$  then yields  $|C|^2 \mathcal{T}_{QD}$ ,  $K$ ,  $z$ ,  $P$  and  $Q$ , and thus  $\cos(\alpha_{QD} + \delta_B + 2|k|a) = P/\sqrt{Q}$ , from which one can extract the  $V$ -dependence of  $\alpha_{QD}$ . The same  $V$ -dependence of  $\alpha_{QD}$  is also contained in  $K \propto (\cot \alpha_{QD} + \cot |k|a)$ . As discussed after Eq. (5), our model also implies that  $\mathcal{T}_{QD} = \gamma_D^2 \sin^2(\alpha_D)$ . Since the  $V$ -dependence of  $\mathcal{T}_{QD}$  can also be extracted from the fitted values of either  $|C|^2 \mathcal{T}_{QD}$  or  $Q$ , we end up with several consistency checks for the determination of  $\alpha_{QD}$ . Additional checks arise from direct measurements of  $\mathcal{T}_{QD}$  and  $\mathcal{T}_B = |t_B|^2$ , by taking the limits  $|V_0| = |\epsilon_0| \rightarrow \infty$  or  $|V| = |\epsilon_D| \rightarrow \infty$ .

The LHS frame in Fig. 7 shows an example of the  $V$ - and  $\phi$ -dependence of  $\mathcal{T}$  for this limit (no interactions), with  $ka = \pi/2$  and  $J_L = J_R = I_L = I_R = 1$ ,  $V_0 = 4$  (in units of  $J$ ), implying  $K = \epsilon_D/\epsilon_0 = V/V_0$ . Far away from the resonance  $\mathcal{T} \ll 1$ ,  $Q \ll |P| \ll 1$  and  $|K| \gg 1$ , yielding the two-slit-like form  $\mathcal{T} \approx A + B \cos \phi$ , dominated by its first harmonic, with  $B/A \approx 2[K^{-1} - P]$ . However, close to the resonance  $\mathcal{T}$  shows a rich structure; the denominator in Eq. (16) generates higher harmonics, and the two-slit formula is completely wrong. This rich structure may be missed if one neglects parts of the  $\phi$ -dependence of  $\Delta$ , as done in parts of Ref. [42]. Note also the Fano vanishing [36] of  $\mathcal{T}$  for  $V \sim 10$  at  $\phi = 2n\pi$ , with integer  $n$ . Without interactions, we can repeat this calculation for a dot with several resonances, using Eq. (7). The RHS frame in Fig. 7 shows results for two resonances, with  $\epsilon_D = \pm 5$ . Interestingly, Fig. 7 is qualitatively similar to the experimentally measured transmission in Ref. [43]. However, so far there has been no quantitative analysis of the experimental data.

To treat the general case, we need information on  $\Delta_{int}$ . First of all, we emphasize that *a successful fit to Eq. (16) justifies the neglect of the  $\phi$ -dependence of  $\Delta_{int}$* . If the various procedures to determine  $\alpha_{QD}$

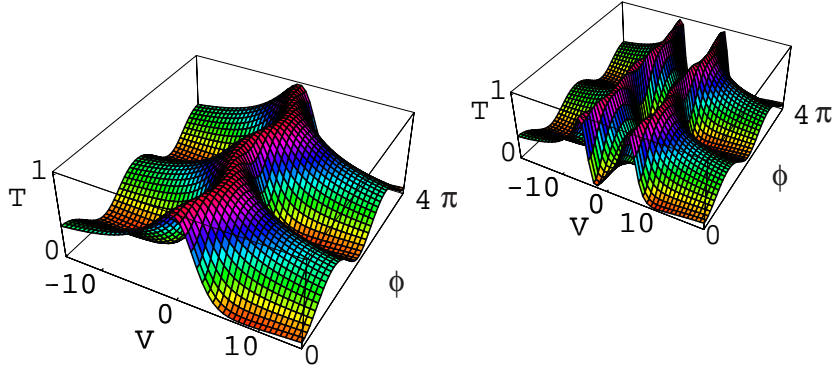


**Figure 7.** AB transmission  $\mathcal{T}$  versus the AB phase  $\phi$  and the gate voltage  $V$ , for one (LHS) and two (RHS) non-interacting resonances.

from Eq. (16) yield the same  $V$ -dependence, this would also confirm that  $\Delta_{int}$  is negligibly small. A failure of this check, or a more complicated dependence of the measured  $\mathcal{T}$  on  $\cos \phi$ , would imply that  $\Delta_{int}$  is not negligible.

As seen from Eq. (14),  $\Delta_{ext}$  is fully determined by a single “visit” of the electron at “ref”. For small  $\mathcal{T}_B$ , or large  $|V_0| = |\epsilon_0|$ , it is reasonable to conjecture that  $\Delta_{int}$  is also dominated by such processes. In that case, we expect  $\Delta_{int}$  to be proportional to the same brackets as in Eq. (14), i.e.  $\Delta_{int} \approx w(z + \cos \phi)$ , with a real coefficient  $w$ . This yields the same dependence of  $\mathcal{T}$  on  $\cos \phi$  as in Eq. (16), with a shifted coefficient  $v$ . If  $w$  depends only weakly on  $V$ , then this shift has little effect on the determination of  $\alpha_{QD}$ . Again, the validity of this approach relies on getting the same  $V$ -dependence of  $\alpha_{QD}$  from all of its different determinations.

## 4. Model for the open AB interferometer

Our model for the open interferometer is represented schematically in Fig. 2(c). In order to obtain explicit expressions, which are easy to calculate, we again neglect interactions, and use a simple tight-binding model [28]. To allow several leaky branches from each edge of the triangle in Fig. 6, we first generalize the closed interferometer model, and replace each such edge  $s$  by a 1D tight binding model of  $M_s$  sites, with  $\epsilon_i = 0$  and  $J_{i,i+1} = J_s$  ( $s = \ell, r, d$  for the left and right upper segments and for the lower path, respectively). Taking advantage of gauge invariance, we attach the AB phase factor  $e^{i\phi}$  to the hopping amplitude from the right hand “fork” onto its nearest neighbor on branch  $r$ , which we write as  $J_r e^{-i\phi}$ . Writing the wave functions in segment  $s$  as  $\psi_m^s = A_s \eta_s^m + B_s \eta_s^{-m}$ , with  $\eta_s$  given by  $E = -J_s(\eta_s + \eta_s^{-1})$ , it is easy to express the total transmission and reflection amplitudes through the interferometer,  $t$  and  $r$ , in terms of the six amplitudes  $\{A_s, B_s\}$ , and obtain six linear equations whose coefficients also contain  $\{S_{XY}\}$ . Having solved these equations, one finally finds the total transmission amplitude  $t$ . Interestingly, the dependence of  $\mathcal{T}$  on  $\phi$  for the closed interferometer remains of the form given in Eq. (16). To obtain the LHS frame in Fig. 3, we used  $M_\ell = M_r = 6$ ,  $M_d = 12$ , and  $J_s = J$ . A fit to Eq. (3) indeed gives that  $\beta$  jumps between 0 and  $\pi$ , as in Yacoby *et al.*’s experiments [8].

We next proceed to model the open interferometer. Pursuing one possible scenario [27], we model the “leaking” from each of the three segments on the “ring” (imitating the additional four terminals in the experiment, Fig. 2(b)) by connecting each site on the three ring segments to a 1D lead, which allows only an outgoing current to an absorbing reservoir (Fig. 2(c)). Each such segment is thus replaced by a “comb” of absorbing “teeth”.

We start by investigating the properties of a single “comb”. The “base” of the “comb” is described by a chain of  $M$  tight-binding sites, with  $J_{m,m+1} = J_c$  and  $\epsilon_m = 0$ . Each “tooth” is represented by a 1D tight-binding chain, with  $\epsilon_j = 0$ . The first bond on the “tooth” has  $J_{m,0} = J_x$ , while  $J_{j,j+1} = J$  for  $j \geq 0$ . Assuming only outgoing waves on the teeth, with wave functions  $t_x e^{ikaj}$  and energy  $E = -2J \cos ka$ , one can

eliminate the “teeth” from the equations. The wave functions on the “base” of the comb are then given by  $\psi_m^c = A_c \eta_c^m + B_c \eta_c^{-m}$ , where  $\eta_c$  is a solution of the (complex energy) equation  $E + J_x^2 e^{ika} / J = -J_c(\eta_c + \eta_c^{-1})$ . When this “comb” is treated as our basic scatterer, i.e. connected via  $J_{in}$  and  $J_{out}$  to our “standard” two leads, then the transmission and reflection amplitudes via the “comb” are given (up to unimportant phases) by  $t = J_{out}(A_c \eta_c^N + B_c / \eta_c^N) / J$  and  $r = J_{in}(A_c \eta_c + B_c / \eta_c) / J - e^{ika}$ , and one ends up with two linear equations for  $A_c$  and  $B_c$ . The results for  $\mathcal{T} = |t|^2$  and  $\mathcal{R} = |r|^2$  are shown, for three values of  $M$ , in Fig. 8, as functions of  $ka \in [0, \pi]$  in the free electron energy band, for  $J_x = .7J$  (left), and as functions of  $J_x$ , for  $ka = \pi/2$  (right). In the figure,  $J_c = J_{in} = J_{out} = J$ . It is rewarding to observe that both  $\mathcal{T}$  and  $\mathcal{R}$  are almost independent of the electron energy  $E$  over a broad range near the band center. It is also interesting to note that for these parameters,  $\mathcal{T}$  decreases with  $J_x$ , but  $\mathcal{R}$  increases with  $J_x$ . For fixed  $J_x$ ,  $\mathcal{T}$  and  $\mathcal{R}$  exhibit some even-odd oscillations with  $M$ , but basically  $\mathcal{T}$  decreases with  $M$  while  $\mathcal{R}$  increases towards an almost constant value for  $M > 6$ . This is understandable: a strong coupling to the “teeth” causes a strong decay of the wave function along the “comb”. Thus, for each value of  $M$  one can find an intermediate optimal region in which both  $\mathcal{T}$  and  $\mathcal{R}$  are small. This region broadens, and has smaller  $\mathcal{T}$  and  $\mathcal{R}$ , for larger  $M$ .

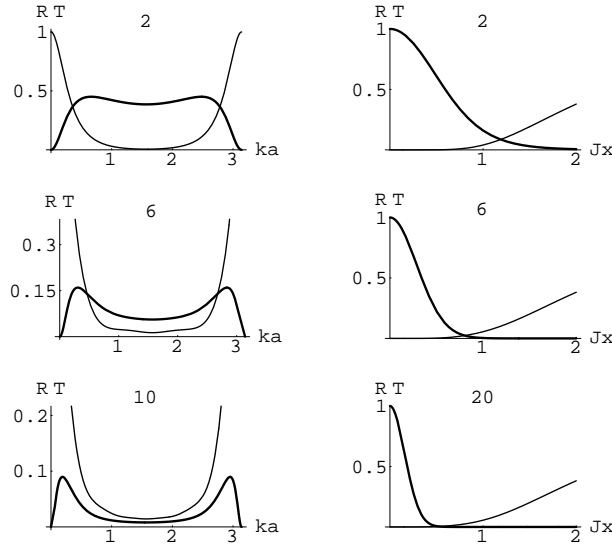


**Figure 8.** Transmission (thick line) and reflection (thin line) through a “comb”, versus  $ka$  at  $J_x = .7J$  (left) and versus  $J_x$  at  $ka = \pi/2$  (right). The number on each frame gives the number of “teeth”,  $M$ .

We next place three such “combs” on the AB interferometer, as in Fig. 2(c), and study the AB transmission  $\mathcal{T}$  as function of the various parameters (for the present purposes, the site “ref” is just equivalent to the other sites on the lower edge, i.e.  $\epsilon_0 = 0$ ). For simplicity, we set the same parameters for all the combs, and vary the coupling strength  $J_x$ . Since each “tooth” of the “comb” can be replaced by adding the complex number  $J_x^2 e^{ika} / J$  to the energy  $E$  in the equations for  $\psi_m^s$  on the ring segments, the mathematics is similar of that of the “bare” closed interferometer. The main difference in the results is that now  $\eta_c$  is complex, yielding a decay of the wave function through each comb. This also turns the ratio  $K$  complex, so that the numerator in Eq. (16) must be replaced by  $|1 + K e^{i\phi}|^2$ , yielding non-trivial values for  $\beta$ . To demonstrate qualitative results, we again choose  $M_\ell = M_r = 6$ ,  $M_d = 12$ , use  $J_\ell = J_r = J_d = J_c = J$  and keep  $ka = \pi/2$  and the QD parameters  $J_L(n) = J_R(n) = J$ ,  $N = 4$ ,  $U = 20J$ . The choice for the “comb” parameters ensures that  $A$  and  $B$  in Eq. (3) are of the same order. Other choices give similar qualitative results. Figure 3 shows results for  $A$ ,  $B$ ,  $C$  and  $\beta$  as function of  $V$ , for several values of  $J_x$ . Clearly,  $J_x = .15J$  gives a phase  $\beta$  which is intermediate between the Onsager jumps of the left Fig. 3 and the exact intrinsic  $\alpha_{QD}$  of Fig. 1. Increasing  $J_x$  yields a saturation of  $\beta$  onto  $\alpha_{QD}$ , which persists for a broad range between  $J_x = .5J$  and  $J_x = .9J$ . However, larger values of  $J_x$ , e.g.  $J_x = 1.5J$ , cause a deviation of  $\beta$  from  $\alpha_{QD}$ , due to the increase of the reflection from each “comb”. Interestingly, this deviation is **in the same direction** as for

small  $J_x$ ! The reason for this is clear: as the reflection of each comb increases, the electron “rattles” in and out of the QD. This localizes it on the QD, and reduces the width of the QD resonances. For these large values of  $J_x$ , one has  $|P|, Q \ll 1$  in Eq. (16). Thus, the two-slit conditions hold, and one has  $B \propto |t_1|$  and  $\beta = \alpha_1$ . We have solved the equations for the transmission through the upper branch only (disconnecting the lower branch altogether), and found that indeed, the coefficient  $c$  in  $t_1 = ct_{QD}$  is a constant as long as the reflection of the combs is small. However, as  $J_x$  increases above about  $.9J$ ,  $c$  is no longer a constant. The narrower resonances shown in Fig. 3 (right) fully agree with this modified upper branch transmission. In any case, “optimal combs”, with small  $\mathcal{T}$  and  $\mathcal{R}$ , do yield  $\beta = \alpha_{QD}$ .

So far, we assumed *no* direct losses from the QD itself. It is easy to add such losses, by connecting a “lossy” channel to each resonant state  $n$  [27], similar to the “teeth” of our “combs”, with a tunneling amplitude  $J'_x$ . As before, this introduces a complex addition  $J_x'^2 e^{ika}$  to  $E - E_R(n)$ . Figure 9 shows the results for the same parameters as above, but with  $J_x = J'_x = .9J$ . Clearly, the new imaginary parts eliminate the Fano-like zero in  $B$ , and yield a smooth variation of  $\beta$  near the “intrinsic phase lapses”. Although similar to the behavior arising in the BW approximation, the present effects are *real*, due to physical breaking of the unitarity on the QD. It is interesting to note that the data of Ref. [9] show similar (and otherwise unexplained) smooth features. It is however possible that the latter come from finite temperature averaging [34].

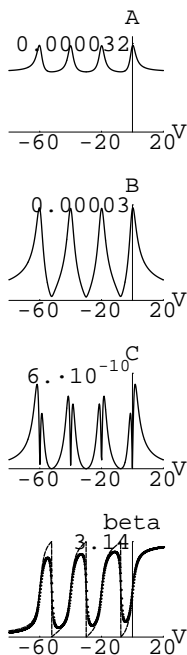


**Figure 9.** Same as Fig. 3, but with a “lossy” channel attached to the QD;  $J_x = J'_x = .9J$ .

## 5. Concluding remarks

Basically, we presented three methods to measure the intrinsic scattering phase of a quantum dot. The first method is based on Eq. (6), and does not involve interferometry. The second is based on Eq. (15), which allows one to extract information from measurements on the closed ABI. The third method uses the open ABI, but requires conditions under which this ABI behaves as a two-slit interferometer. As stated, a convincing approach would be to use more than one method, with the same QD, and to obtain consistent results.

The actual plots shown in this paper were obtained with simple tight-binding models, without interactions

(except for simple Hartree-like terms in the single electron energy). Therefore, these plots cannot be used for the strongly interacting case, particularly in the Kondo regime. Although some aspects of the interacting case have been included in our analysis for the single QD or for the closed ABI, the full inclusion of interactions in practical calculations remain an open problem.

In addition to electron-electron interactions, one might also consider the effects of other interactions. We have recently studied the interactions of the electrons with a phonon bath, which acts only on the QD (still embedded on one path of the closed ABI). The persistent current  $I_p$  around the “ring”, at steady state, is found to be enhanced in an appropriate range of the intensity of the acoustic source [44].

## Acknowledgements

We thank B. I. Halperin, M. Heiblum, Y. Levinson, A. Schiller, H. A. Weidenmüller and A. Yacoby for helpful conversations. This project was carried out in a center of excellence supported by the Israel Science Foundation, with additional support from the Albert Einstein Minerva Center for Theoretical Physics at the Weizmann Institute of Science, and from the German Federal Ministry of Education and Research (BMBF) within the Framework of the German-Israeli Project Cooperation (DIP).

## References

- [1] L.P. Kouwenhoven *et al.*, *Mesoscopic Electron Transport*, NATO Advanced Study Institute, Series E: Applied Science, Vol. **345**, edited by L. L. Sohn, L. P. Kouwenhoven and G. Schön (Kluwer, Dordrecht, 1997), p. 105.
- [2] Y. Imry, *Introduction to Mesoscopic Physics* (Oxford University Press, Oxford 1997; 2nd edition, 2002).
- [3] M.A. Kastner, *Physics Today*, **46**(1), (1993) 24.
- [4] J. Friedel, *Can. J. Phys.*, **34**, (1956), 1190.
- [5] D.C. Langreth, *Phys. Rev.*, **150**, (1966), 516.
- [6] A. C. Hewson, *The Kondo Problem for Heavy Fermions* (Cambridge University Press, Cambridge 1997).
- [7] R. Landauer, *Phil. Mag.*, **21**, (1970), 863.
- [8] A. Yacoby, M. Heiblum, D. Mahalu and H. Shtrikman, *Phys. Rev. Lett.*, **74**, (1995), 4047.
- [9] R. Schuster *et al.*, *Nature*, **385**, (1997), 417.
- [10] Y. Gefen, Y. Imry and M. Ya. Azbel, *Phys. Rev. Lett.*, **52**, (1984), 129.
- [11] e. g. R.P. Feynmann, R.B. Leighton and M. Sands, *The Feynmann Lectures on Physics*, Vol. III, Chap. 1 (Addison-Wesley, Reading 1970).
- [12] Y. Aharonov and D. Bohm, *Phys. Rev.* **115**, (1959), 485.
- [13] A. Tonomura, *Electron Holography*, 2nd ed. (Springer, Heidelberg, 1999).
- [14] R.A. Webb, S. Washburn, C.P. Umbach and R.B. Laibowitz, *Phys. Rev. Lett.*, **54**, (1985), 2696.
- [15] L. Onsager, *Phys. Rev.*, **38**, (1931), 2265; H.B.G. Casimir, *Rev. Mod. Phys.*, **17**, (1945) 343.
- [16] M. Büttiker, *Phys. Rev. Lett.*, **57**, (1986) 1761.
- [17] A. Aharony, O. Entin-Wohlman and Y. Imry, *Phys. Rev. Lett.*, **90**, (2003), 156802.
- [18] J. Wu *et al.*, *Phys. Rev. Lett.*, **80**, (1998), 1952.
- [19] K. Kang, *Phys. Rev. B*, **59**, (1999), 4608.
- [20] G. Hackenbroich and H. A. Weidenmüller, *Europhys. Lett.*, **38**, (1997), 129.

- [21] Y. Oreg and Y. Gefen, *Phys. Rev. B*, **55**, (1997), 13726.
- [22] C.-M. Ryu and Y.S. Cho, *Phys. Rev. B*, **58**, (1998), 3572.
- [23] H. Xu and W. Sheng, *Phys. Rev. B*, **57**, (1998), 11903.
- [24] H.-W. Lee, *Phys. Rev. Lett.*, **82**, (1999), 2358.
- [25] P.G. Silvestrov and Y. Imry, *Phys. Rev. Lett.*, **85**, (2000), 2565.
- [26] A. Levy Yayati and M. Büttiker, *Phys. Rev. B*, **62**, (2000), 7307.
- [27] O. Entin-Wohlman, A. Aharony, Y. Imry, Y. Levinson and A. Schiller, *Phys. Rev. Lett.*, **88**, (2002), 166801.
- [28] A. Aharony, O. Entin-Wohlman, B.I. Halperin and Y. Imry, *Phys. Rev. B*, **66**, (2002), 115311.
- [29] T.K. Ng and P.A. Lee, *Phys. Rev. Lett.*, **61**, (1988), 1768.
- [30] O. Entin-Wohlman, C. Hartzstein and Y. Imry, *Phys. Rev. B*, **34**, (1989), 921.
- [31] J.L. d'Amato, H.M. Pastawski and J.F. Weitz, *Phys. Rev. B*, **39**, (1989), 3554.
- [32] D. Kowal, U. Sivan, O. Entin-Wohlman and Y. Imry, *Phys. Rev. B*, **42**, (1990), 9009.
- [33] We assume zero temperature, so that  $E$  is equal to the Fermi energy. Finite temperature replaces the sharp “phase lapses” by smooth but fast changes [34].
- [34] Q. Sun and T. Lin, *Euro. Phys. Jour. B*, **5**, (1998) 913.
- [35] U. Fano, *Phys. Rev.*, **124**, (1961), 1866.
- [36] O. Entin-Wohlman, A. Aharony, Y. Imry, and Y. Levinson, *J. Low Temp. Phys.*, **126**, (2002), 1251.
- [37] J. Göres *et al.*, *Phys. Rev. B*, **62**, (2000) 2188.
- [38] G. Breit and E. Wigner, *Phys. Rev.*, **49**, (1936) 519.
- [39] Y. Ji, M. Heiblum, D. Sprinzak, D. Mahalu, and H. Shtrikman, *Science*, **290**, (2000), 779.
- [40] H.A. Weidenmüller, *Phys. Rev. B*, **65**, (2002), 245322.
- [41] K.A. Matveev, *Phys Rev. B*, **51**, (1995), 1743.
- [42] W. Hofstetter, J. König and H. Schoeller, *Phys. Rev. Lett.*, **87**, (2001), 156803.
- [43] K. Kobayashi, H. Aikawa, S. Katsumoto, and Y. Iye, *Phys. Rev. Lett.*, **88**, (2002), 256806.
- [44] O. Entin-Wohlman, Y. Imry and A. Aharony, *Phys. Rev. Lett.*, **91**, (2003), 046802; cond-mat/0302146.